International Applied Mechanics, Vol. 41, No. 3, 2005

DEVELOPING A COMPRESSIVE FAILURE THEORY FOR NANOCOMPOSITES

A. N. Guz[1], A. A. Rodger[2], and I. A. Guz[2]

UDC 539.3

The paper addresses a compressive-failure theory for polymer-matrix nanocomposites in the case where failure onset is due to microbuckling. Two approaches based on the three-dimensional linearized theory of stability of deformable bodies are applied to laminated and fibrous nanocomposites. According to the first approach (continuum compressive-failure theory), nanocomposites are modeled by a homogeneous anisotropic medium with effective constants, including microstructural parameters. The second approach uses the piecewise-homogeneous model, three-dimensional relations for fibers (CNT) and matrix, and continuity conditions at the fiber–matrix interface. The compressive-failure theory is used to solve specific problems for laminated and fibrous nanocomposites. Some approximate failure theories based on the one- and two-dimensional applied theories of stability of rods, plates, and shells are analyzed

Keywords: nanocomposites, CNT fiber, polymer matrix, compressive failure, microbuckling, three-dimensional linearized theory of stability of deformable bodies

Introduction. Today's literature on the fracture mechanics of composites considers the paper [17] to be the first to describe, in 1960, fiber microbuckling as a compressive failure mechanism for unidirectional fibrous composites. In the years that followed, several authors set forth different approximate models for the quantitative and qualitative description of this mechanism. These models are based on a number of assumptions and hypotheses, of which the following are worth mentioning: no (neglected) subcritical stresses in the matrix, use of applied one- and two-dimensional theories of stability of rods and plates to study microbuckling, modeling of the matrix by a one-dimensional elastic object, etc.

The paper [14] was apparently the first to propose, in 1965, a highly approximate model for the quantitative description of microbuckling in composites within the framework of a plane problem (in fact, the fibrous composite was modeled by a laminated composite), using the above-mentioned assumptions and hypotheses (the same results were reported in [14]). Despite the highly approximate model, the results from [14] were used in many publications, including the seven-volume collective monograph [13], and are generally recognized and widely cited. In the literature on the fracture mechanics of composites (see, e.g., [15]), these results are named the Dow–Gruntfest–Rosen–Schuerch theory, after the authors of the first publications [14, 17, 45, 46].

Thus, to describe the failure mechanism in question [17], we need a stability theory for unidirectional fibrous composites (Fig. 1) or laminated composites (Fig. 2) subjected to axial compression. The paper [17] addressed a fibrous composite; thus, it is expedient to construct a stability theory for the material represented in Fig. 1. In this connection, a stability theory for laminated composites (Fig. 2) is to be developed to attain two ends (two different cases). In the first case, a stability theory is needed to describe the failure mechanism for compressed laminated composites, which is likely to be related to the failure mechanism for compressed fibrous composites observed in [17]. Moreover, structural elements made of fibrous composites are formed as a laminated composite whose layers, which are monolayers of a unidirectional fibrous material, are

[1]S. P. Timoshenko Institute of Mechanics, National Academy of Sciences of Ukraine, Kiev. [2]University of Aberdeen, Scotland. Translated from Prikladnaya Mekhanika, Vol. 41, No. 3, pp. 3–37, March 2005. Original article submitted December 29, 2004.

1063-7095/05/4103-0233

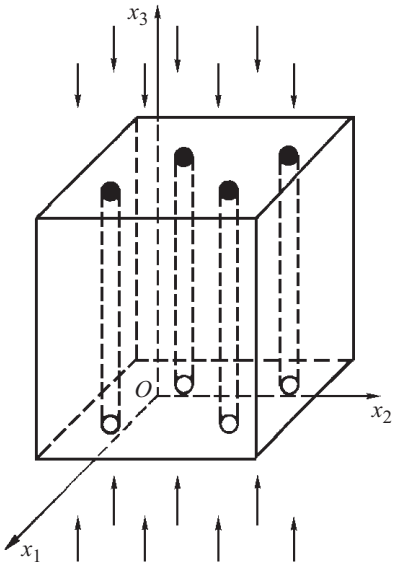

Fig. 1

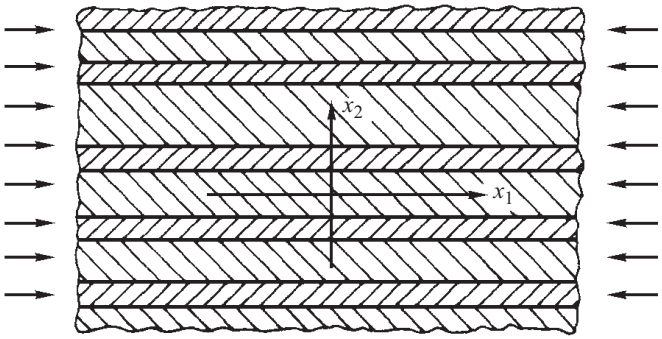

Fig. 2

stacked so that the fibers of neighboring layers are directed at a certain angle to each other. In the second case, a stability theory for laminated composites is needed to describe the failure mechanism for the initial compressed unidirectional fibrous composite, with a plane problem model applied to fibrous composites. Such an approach was implemented in [14], where the failure mechanism for fibrous composites was analyzed within the framework of the plane problem for laminated composites. It should be noted that the fibers in a fibrous composite (Fig. 1) interact in much more complex fashion than in a laminated composite (Fig. 2). Hence, an analysis of the failure mechanism within the framework of the plane problem for laminated composites cannot reveal all features of the failure mechanism for fibrous composites, which is primarily true of the results from [14].

It should also be noted that an analysis of complex phenomena in solid mechanics would produce reliable and accurate data only if the three-dimensional formulation was used. Since the phenomenon under consideration [17] is rather complex and pertains to the stability of nonthin bodies, reliable and accurate data can be obtained using the three-dimensional linear theory of stability of deformable bodies (see, e.g., [4, 6, 19, etc.]).

Independently of and almost simultaneously with [14], the papers [2, 3], published in 1969, proposed to describe the failure mechanism [17] or related failure mechanisms or microbuckling using the three-dimensional linear theory of stability of deformable bodies (TLTSDB). The results based on [2, 3] were extended in [7] to fibrous (Fig. 1) and laminated (Fig. 2) composites of various structures with polymer matrix (modeled by a linear elastic body) and metal matrix (modeled by an elastoplastic body), with the generalized concept of continuous loading [6, 19] applied in the latter case. In fact, the papers [2, 3] proposed two approaches, each based on the TLTSDB [4, 6, 19], for modeling composites taking their microstructure into account. The first approach [2] employs the continuum approximation where a homogeneous anisotropic body with effective constants (homogenized) is used as a model. The parameters characterizing the composite microstructure appear in the expressions for the effective constants of the homogeneous anisotropic body. With such an approach, the theoretical compressive strength and the nature of failure (propagation of fracture) are determined from an analysis of internal or surface instability (transition of the governing system of equations from elliptic to hyperbolic) and related situations. The results obtained in [7] concern the internal failure of composites (failure of the whole sample or a structural element) or the surface failure of composites (failure of near-surface layers) under uniaxial, biaxial, and triaxial compression. The second approach [3] employs the piecewise-homogeneous model, where the TLTSDB is applied separately to the reinforcement (fibers and layers) and to the matrix (see, e.g., [4, 6, 19]), with continuity conditions for stresses and displacements satisfied at the reinforcement–matrix interface. The second approach is certainly more accurate; therefore, the results it produces may be used to estimate the results obtained by the first approach and by other approximate (including highly approximate) models [14]. It should be noted that the results produced by the approach [3] and reported in [7] are exactest among those that can be obtained in

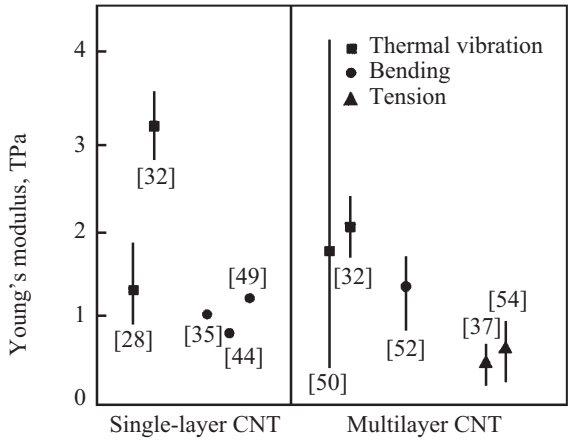

Fig. 3

solid mechanics. In this situation, the results from [7] can only be improved by refining the matrix–reinforcement interface conditions and the equations of state describing the properties of the reinforcement and matrix.

In succeeding years, the approach [2, 3, 7] was used to construct a failure theory for composites with interfacial cracks (see [9–12, 21, 24] and references therein). The corresponding exact solutions were analyzed in [22]. The approach [2, 3, 7] was also used to develop the two-level theory of compressive failure near stress concentrators in composites. The first results in this area were reported in [5] and analyzed in [20].

Constructing a compressive-failure theory for composites based on the microbuckling mechanism is a nonclassical problem of fracture mechanics. Some other nonclassical problems of fracture mechanics were analyzed in [8].

The above-mentioned results pertain to the mechanics (including micromechanics) of composites, which actively developed in the second half of the 20th century. The late 20th century and the early 21st century witnessed the creation and investigation of carbon nanotubes (CNT). Some approaches to problems of nanomechanics and mechanics of nanocomposites were addressed in [23]. Since CNTs are of high modulus and high strength, they may potentially be used as a reinforcement in nanocomposites.

Considering the aforementioned, we will address a compressive-failure theory for polymer-matrix nanocomposites developed based on the microbuckling mechanism and the three-dimensional linear theory of stability of deformable bodies (see, e.g., [2–4, 6, 7, 19]).

1. Properties of CNT-Reinforcement and Polymer Matrix. In this section, we will briefly analyze some data on the mechanical properties of CNTs and polymer matrix needed for further discussion.

1.1. Mechanical Properties of CNT. There are a great number of publications on the mechanical properties of single- and multi-layer CNTs. These properties have been determined both theoretically and experimentally (see [30, 38, 41, 47, 54, etc.] for reviews of the results obtained in the area).

Figure 3 (borrowed from [54, p. 978]) shows Young's modulus E (TPa = 1000 GPa) for single-layer CNTs (the left-hand half of the figure) and for multilayer CNTs (the right-hand half of the figure). These results have been obtained using three experimental methods: thermal vibration (■), bending (●), and tension (▲). The numbers in square brackets indicate the publications (see References herein) where the corresponding value was reported (the numbers in square brackets in [54, p. 978] refer to publications in the list of references therein). From Fig. 3 it follows that Young's moduli (measured along the CNT-axis) of single- and multi-layer CNTs differ insignificantly (which confirms that the results pertain to a nanotube material) and that Young's moduli experimentally determined by other authors differ significantly. In this connection, there is good reason to use the following mean Young's modulus to evaluate the theoretical compressive strength for CNTs:

$$E \approx (1.00–1.20) \text{ TPa}. \tag{1}$$

Today's scientific literature includes more theoretical data on Young's modulus for nanotubes than experimental. Moreover, theoretical methods have made predictions on a wider range of mechanical properties. An example is the theoretical results obtained in [30] by the method of molecular dynamics simulations for single-, two-, and three-layer CNTs with

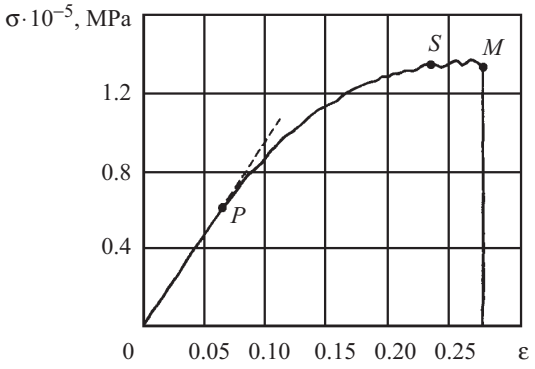

Fig. 4

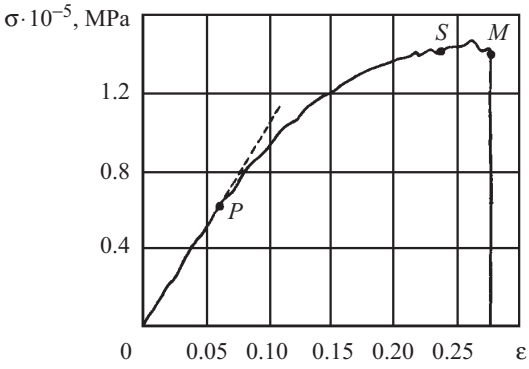

Fig. 5

TABLE 1

Chirality	Young's modulus	
	[30]	other authors
(4, 4)	55.3	56.4
(7, 0)	55.7	56.3
(7, 7)	56.0	56.5
(12, 0)	56.4	55.2

$LD^{-1} = 4.5$ and $LD^{-1} = 9.1$ (L and D are the CNT length and diameter). The publication [30, pp. 2523, 2524] also presents uniaxial-tension curves (σ versus ε) such as those in Fig. 4 for four-layer CNT of chirality (5, 5), (10, 10), (15, 15), and (20, 20) ($LD^{-1} = 4.5$) and in Fig. 5 for single-layer CNT of chirality (10, 10) ($LD^{-1} = 9.1$). In Figs. 4 and 5, the points R, S, and M correspond to the elastic limit, yield stress, and failure stress, respectively. Since the curves in Figs. 4 and 5 are nonlinear, the CNTs are concluded in [30] to have plastic properties. This conclusion requires further checking, since only the case of active loading has been examined, leaving unloading aside. The results from [30] agree well with those obtained by other authors (see Table 1 [30, p. 2523], which compares dimensionless Young's moduli for single-layer CNTs of different chirality with $LD^{-1} = 9.1$).

According to Figs. 4 and 5, we introduce the following notation: the elastic limit σ_l and the corresponding strain ε_l (point P), the yield stress σ and the corresponding strain ε (point S), the ultimate (failure) stress $\sigma_{str} = \sigma_{fr}$ and the corresponding strain ε_{fr} (point M), and the maximum elastic strain ε_{el}^{max}. This notation is used in Table 2 (borrowed from [30, p. 2525]) collecting mechanical properties of different CNTs. Table 2 also contains the values of A and B appearing in the nonlinear relation

$$\sigma = (A\varepsilon + B)\varepsilon, \quad \varepsilon_1 \le \varepsilon \le \varepsilon_{yield}, \tag{2}$$

and describing deformation due to uniaxial tension between the elastic limit σ_1 and the yield point σ_T.

From Table 2 [30], it follows that:

(i) Young's moduli for single-, two-, three-, and four-layer CNTs differ insignificantly;

(ii) Young's moduli for relatively short CNTs ($LD^{-1} = 4.5$) and relatively long CNTs ($LD^{-1} = 9.1$, twice longer) differ insignificantly;

(iii) the "mean" Young's modulus is defined by expression (1) derived to analyze the experimental results in [54]; and

(iv) the relationship between stresses and strains under uniaxial tension is linear while $\varepsilon \le 6\%$.

In the case of axial compression, according to [52], the stress–strain relationship is linear while the strain is less than 5%.

TABLE 2

CNTs	$\frac{L}{D}$	E, TPa	$\sigma_1 \cdot 10^{-4}$, MPa	$\sigma_{yield} \cdot 10^{-5}$, MPa	$\sigma_{fr} \cdot 10^{-5}$, MPa	$\varepsilon_1 \cdot 10$	ε_{el}^{max}	ε_{fr}	A, TPa	B, TPa
Single-layer (10, 10)	4.5	1.043	6.103	1.369	1.404	0.585	0.231	0.280	–2.625	1.211
	9.1	1.031	6.271	1.421	1.485	0.594	0.236	0.279	–2.522	1.190
Two-layer (5, 5) and (10, 10)	4.5	1.161	7.231	1.614	1.624	0.627	0.247	0.279	–2.543	1.259
	9.1	1.175	7.287	1.633	1.685	0.621	0.242	0.281	–2.810	1.362
Three-layer (5, 5), (10, 10) and (15, 15)	4.5	1.000	6.068	1.430	1.434	0.605	0.238	0.281	–2.358	1.160
	9.1	0.972	5.645	1.381	1.414	0.611	0.246	0.282	–2.275	1.120
Four-layer (5, 5), (10, 10), (15, 15), and (20, 20)	4.5	0.932	6.075	1.343	1.382	0.654	0.235	0.281	–2.234	1.103
	9.1	0.872	5.784	1.278	1.327	0.633	0.241	0.280	–2.132	1.023

Along with experimental values of axial Young's moduli for CNTs, the publication [54] discusses Young's moduli determined by different theoretical methods. Figure 6 (borrowed from [54, p. 980]) shows Young's modulus (in TPa = 1000 GPa) obtained theoretically by different authors for single-layer CNTs (the left-hand half of the figure) and for multilayer CNTs (the right-hand half of the figure). These results have been obtained by three different methods (see the upper portion of the figure for the method names and the symbols representing them). The numbers in square brackets indicate the publications (see References herein) where the corresponding value was reported (the numbers in square brackets in [54, p. 980] refer to publications in the list of references therein). From Fig. 6, it follows that Young's moduli E (measured along the CNT-axis) for single- and multi-layer CNTs differ insignificantly and that Young's moduli obtained theoretically by other authors differ significantly. In this connection, there is good reason to use the mean Young's modulus (1) to evaluate the theoretical compressive strength for CNTs.

We have briefly discussed mechanical properties of CNTs. The results cited above indicate that Poisson's ratios ν for CNT have been studied inadequately. Therefore, we cannot adequately investigate (in developing a compressive-failure theory for nanocomposites) the influence of the difference between Poisson's ratios of the matrix and CNT on the failure mechanisms under consideration.

Since we are addressing nanocomposites, the failure mechanisms depend not only on the mechanical properties of CNTs but also on their geometry. In this connection, we will briefly discuss the geometrical parameters of CNTs, namely thickness and diameter. The geometry of CNTs was partially described in [23] and references therein. Let us consider some of these results, using the following notation: D for diameter, L for length, and h for thickness. The minimum diameter of single-layer CNTs mentioned in the literature is $D = 0.4$ nm (the carbon atom's diameter is considered about 0.15 nm). Thus, the carbon atoms in 0.4-nm CNT may be thought of as interacting not only along the CNT surface but also along the diameter. In this connection, after continualization [23], such CNTs can be modeled by a circular solid cylinder with $D = 0.4$ nm. This case is the exception rather than a rule for CNTs. In most cases, CNTs are expediently modeled (continuum approximation) by a hollow circular cylinder. Multilayer CNTs described in the literature have $D \approx 4$–30 nm. Note that CNTs can be very long: $LD^{-1} \approx 1000$. Ensembles of CNTs may have diameters $D \approx 30$–50 nm and can be very long ($LD^{-1} \approx 1000$). CNTs can form nanoropes with $D \approx 10$–20 nm, which can also be very long ($LD^{-1} \approx 1000$). Obviously, CNTs, ensembles, and nanoropes may be modeled by infinite circular cylinders. For multilayer CNTs, a more adequate model is an infinite hollow circular cylinder.

Today, relatively short single- and multi-layer CNTs are actively studied too. As already mentioned, extensive data on relatively short CNTs ($LD^{-1} = 4.5, 9.1$) can be found in [30].

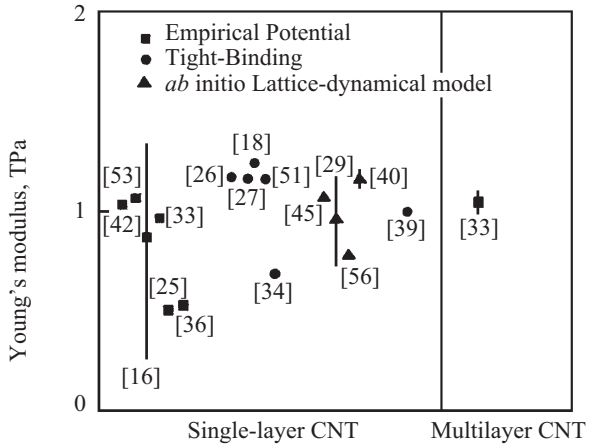

Fig. 6

Let us analyze some recent results from the estimation of the thickness of single- and multi-layer CNTs. For example, the following values of CNT thickness were reported in [30]: h = 0.335 nm for single-layer (10, 10) CNTs, h = 0.67 nm for two-layer (5, 5) and (10, 10) CNTs; h = 1.005 nm for three-layer (5, 5), (10, 10), and (15, 15) CNTs; and h = 1.34 nm for four-layer (5, 5), (10, 10), (15, 15), and (20, 20) CNTs. These are close to the thicknesses of single- and multi-layer CNTs determined by other authors.

Though the published data on the mechanical properties and geometry of CNTs are few in number, we can nevertheless use them to develop a failure theory for nanocomposites.

1.2. Mechanical Properties of Polimer Matrix. The mechanical properties of polymer matrix (different polymer compounds) may be thought of as well understood. They were studied during the creation and investigation of traditional composite materials. We will hereafter consider only brittle and quasibrittle compressive failure involving microbuckling [17]. In this connection, the mechanical properties of the matrix at the elastic stage of deformation will be of our main interest.

Polymeric matrices exhibit the following properties: viscoelastic deformation under long-term external loads and essential temperature dependence of the mechanical properties at relatively high temperatures. These properties may be neglected for two reasons:

(i) since we study the phenomenon of buckling under certain level of load (at certain temperature and viscous strains), we can fix mechanical properties (at certain temperature and viscous strains) and examine the bifurcation buckling mode using the elastic model with such mechanical properties, i.e., so to speak an "instantaneous" elastic model; and

(ii) the use of the elastic model may be attributed to the cases of short-term external loads (the effect of viscous strains is insignificant) and moderate temperatures (the temperature dependence of mechanical properties is insignificant).

In both situations described in (i) and (ii), the buckling process is studied in much the same way, using the elastic model. We use such an approach here to develop a compressive-failure theory for polymer-matrix nanocomposites. Let us now briefly analyze data on the elastic properties of polymer matrices.

Table 3 collects the values of E, σ_l, v, and ε_{fr} for the most-used polymer matrices (the data from Table 3 can be found in [7] and many other publications). The table demonstrates that the values of E, v, σ_l, and ε_{max} are somewhat different for different matrices. Therefore, in evaluating the theoretical compressive strength (while developing a compressive-failure theory), it is appropriate to use the following mean values of Young's modulus and Poisson's ratios, according to [7, p. 30]:

$$E \approx 3.5 \text{ GPa}; \qquad v = 0.4. \tag{3}$$

Note that the mean Young's modulus (1) introduced in the previous section is based on other considerations.

This concludes our discussion of the mechanical properties of CNTs (as potential reinforcements) and polymer matrices as applied to the compressive failure of nanocomposites with microbuckling as a failure mechanism.

2. Fundamentals of Compressive-Failure Theory for Nanocomposites. Let us discuss the fundamentals of failure theory for unidirectional fibrous nanocomposites (Fig. 1) and laminated nanocomposites (Fig. 2) subject to axial compression along fibers and layers. Let the reinforcement be single- or multi-layer CNTs that are quite long, i.e., they can be modeled by

TABLE 3

Matrix	E, GPa	σ_l, MPa	ν	ε_{fr}, %
Epoxy	2.80–4.20	28–91	0.34–0.40	2.6
Polyester	2.10–4.60	42–70	0.35–0.42	< 6
Phenolformaldehyde	2.80–4.60	42–63	0.35	1.5–2
Organic silicon	2.90–4.00	28–35	—	—
Epoxy phenolic-butyral	3.50	41.0	0.40	2.5
Epoxy aniline furfural	5.10	120	0.40	2.5–3
Epoxy maleic	3.15	75	0.38	2.2–2.5

infinite circular cylinders. Such a modeling is acceptable due to the values of LD^{-1} cited at the end of Sect. 1.1. For laminated nanocomposites (Fig. 2), we will consider two cases of result interpretation mentioned at the beginning of Introduction. Following [7], we will use the subscripts "r" and "m" to refer to reinforcement (CNT) and matrix, respectively. We will consider brittle or quasibrittle fracture in the form of microbuckling. The reinforcement and polymer matrix will be modeled by elastic bodies, taking into account the two considerations stated in Sect. 1.2.

We will also assume that Poisson's ratios of the reinforcement and matrix are equal:

$$\nu_r = \nu_m. \tag{4}$$

For laminated nanocomposites, assumption (4) is not needed. For fibrous unidirectional nanocomposites (Fig. 1), assumption (4) substantially simplifies the formulation and solution of problems by making the subcritical stress–strain state homogeneous. In this case, using the three-dimensional linear theory of stability of deformable bodies [4, 6, 19] leads to eigenvalue problems for partial differential equations with constant coefficients in the corresponding coordinate systems, and we can employ the general solutions [4, 6, 19] produced by this theory.

Assumption (4) is appropriate for two reasons:

(i) it, in fact, disregards mechanical effects or quantities of the order of the difference of Poisson's ratios of reinforcement and matrix (ν_r–ν_m) compared to unity (these effects may be considered secondary and can be accounted for later); and

(ii) as already mentioned in Sect. 1.1, there have been only isolated data on Poisson's ratios for CNT (ν_r) published in the scientific literature; therefore, neither the compressive-failure theory for nanocomposites nor any other theory of the mechanics of nanocomposites can produce quantitative results when reliable values of ν_r are needed.

Let us now address the development of the compressive-failure theory for fibrous (Fig. 1) and laminated (Fig. 2) nanocomposites based on the approaches from [2, 3], the TLTSDB [4, 6, 19], and the results from [7] (and references therein). In formulating and solving specific problems, we will take into account the considerations stated at the beginning of this section.

2.1. Continuum Approximation. Let us analyze the results obtained in modeling, according to [2], a nanocomposite by a homogeneous anisotropic elastic body with effective constants. The Cartesian coordinate axes in Figs. 1 and 2 coincide with the axes of symmetry of the composites. In this case, the nanocomposites are modeled by a homogeneous orthotropic elastic body. Since the orthotropic materials are loaded (axially compressed) along their axes of symmetry, the most probable and apparently unique failure mechanism is microbuckling. Here we have a complete analogy with the mechanics of structural members axially compressed along the axis of symmetry, where structural failure is due to buckling.

We will consider a nanocomposite compressed along the axis of symmetry. Its failure will be associated with microbuckling in continuum approximation. The TLTSDB will be used. All these constitute the approach from [2, 7]. Thus, the

onset of failure can be identified with the moment in the loading history when the governing system of equations [4, 6, 19] ceases to be elliptic and becomes hyperbolic. The theoretical compressive strength is also determined from this condition, and fracture propagates along the characteristic planes and surfaces. According to the approach [2, 7], the theoretical compressive strength (resistance to compression along the Ox_i-axis) is defined by*

$$(\Pi_i^-)_T = \langle G_{ij} \rangle, \qquad i \neq j, \tag{5}$$

where $(\Pi_i^-)_T$ is the theoretical compressive strength, and $\langle G_{ij} \rangle$, for $i \neq j$, is the effective shear modulus for an orthotropic homogeneous material with effective constants. In this case, fracture turns out to propagate at an almost right angle to the loading direction. Let us now concretize the above results for unidirectional fibrous and laminated nanocomposites.

2.1.1. Laminated Nanocomposites. Continuum Approximation. According to Fig. 2, we are dealing with a plane problem (plane x_1Ox_2) for laminated nanocomposites compressed along the Ox_1-axis. Therefore, from (5) we obtain

$$(\Pi_1^-)_T = \langle G_{12} \rangle. \tag{6}$$

Substituting the well-known expression for $\langle G_{12} \rangle$ into (6), we obtain [7] a relation for the theoretical compressive strength:

$$(\Pi_1^-)_T = G_\mathrm{r} G_\mathrm{m} (S_\mathrm{r} G_\mathrm{m} + S_\mathrm{m} G_\mathrm{r})^{-1}, \tag{7}$$

where G_r and G_m are the shear moduli of the reinforcement and matrix and S_r and S_m are the volume concentrations of the reinforcement and matrix.

If additionally (4), then (7) turns into

$$(\Pi_1^-)_T = G_\mathrm{m} S_\mathrm{m}^{-1} \left(1 + \frac{S_\mathrm{r}}{S_\mathrm{m}} \frac{E_\mathrm{m}}{E_\mathrm{r}} \right)^{-1}, \qquad G_\mathrm{m} = \frac{E_\mathrm{m}}{2(1+\nu_\mathrm{m})}. \tag{8}$$

Expressions (7) and (8) enable us to evaluate the contraction along the Ox_1-axis (Fig. 2) at failure. According to Fig. 2, the subcritical (from the standpoint of stability theory) deformation of laminated nanocomposite is such that

$$\langle \varepsilon_{11}^0 \rangle = \varepsilon_{11}^{0\mathrm{r}} = \varepsilon_{11}^{0\mathrm{m}} = \langle \varepsilon_\mathrm{fr} \rangle, \tag{9}$$

where $\langle \varepsilon_{11}^0 \rangle$ is the microbuckling strain of the nanocomposite along the Ox_1-axis (Fig. 2), $\varepsilon_{11}^{0\mathrm{r}}$ and $\varepsilon_{11}^{0\mathrm{m}}$ are the microbuckling strains of the reinforcement (CNT) and matrix along the Ox_1-axis (Fig. 2), and $\langle \varepsilon_\mathrm{fr} \rangle$ is the failure strain. Note that the microbuckling is the beginning of the failure process, according to the failure mechanism under consideration.

Young's modulus $\langle E_1 \rangle$ measured along the Ox_1-axis can easily be determined from the equilibrium condition using the homogeneous orthotropic model with effective constants:

$$\langle E_1 \rangle = S_\mathrm{r} E_\mathrm{r} + S_\mathrm{m} E_\mathrm{m}, \tag{10}$$

where E_r and E_m are Young's moduli of the reinforcement (CNT) and polymer matrix. By virtue of (4), transverse effects in nanocomposites are accounted for approximately. In this connection, we will adopt a one-dimensional model to approximate $\langle \varepsilon_\mathrm{fr} \rangle$. Thus, we can determine $\langle \varepsilon_\mathrm{fr} \rangle$ from (8)–(10) for the mean mechanical properties of the reinforcement and matrix (1), (3), (4). Table 4 collects the values of the limit strain corresponding to the theoretical compressive strength (8) for $5 \le S_\mathrm{r} \le 50\%$ (S_r is the CNT concentration). According to Table 4, we have

$$\langle \varepsilon_\mathrm{fr} \rangle < 1\% \quad \text{for} \quad S_\mathrm{r} \ge 15\%. \tag{11}$$

---

* From here on, we will omit the minus sign of the theoretical compressive strength and corresponding limit strain, which are always negative.

TABLE 4

S_r, %	5	10	15	20	25	30	40	50
$\langle \varepsilon_{fr} \rangle$, %	2.4	1.4	0.98	0.78	0.67	0.59	0.52	0.50

From Table 3, it follows that the strain ε_l corresponding to σ_l is somewhat greater than 1% for the overwhelming majority of matrices and is 1.5% and even 2% for some types of matrices. As already mentioned in Sect. 1.1, the stress–strain relationship for axially compressed CNTs considered in [52] remains linear while the strains are less than 5%. This means that the stress–strain relationship for CNTs and polymeric matrices is linear when the strains induced by axial compression are of order 1% (condition (11)). Thus, the principal conclusion is that elastic linear models can be applied to study microbuckling as a compressive failure mechanism for nanocomposites.

It should be noted that this conclusion has been drawn from an analysis of a plane problem for a laminated nanocomposite. Actually, we are considering the failure mechanism [17] for a fibrous nanocomposite, and the plane problem for laminated nanocomposites is inadequate to fibrous nanocomposites. This situation has already been discussed in Introduction, and, obviously, the conclusion formulated above calls for further study on the basis of a model for fibrous nanocomposites (Fig. 1). As already mentioned in Introduction, a fibrous composite was modeled by a laminated composite in [14], and these results have been generally recognized, though they had been obtained using a highly approximate model. Here, we are also considering results from a plane problem for laminated composites obtained based on the TLTSDB and continuum approximation. Let us now compare these results and those from [14].

The analytical results from [14] are fundamental in the Dow–Gruntfest–Rosen–Schuerch theory. Using the notation adopted above, we can express the theoretical compressive strength found in [14] as

$$(\Pi_1^-)_{T[14]} = G_m S_m^{-1}. \tag{12}$$

Comparing expression (8) corresponding to the continuum theory under consideration and expression (12) corresponding to the Dow–Gruntfest–Rosen–Schuerch theory, we draw the following three conclusions.

1. The following inequality always holds:

$$(\Pi_1^-)_T < (\Pi_1^-)_{T[14]}. \tag{13}$$

Hence, the Dow–Gruntfest–Rosen–Schuerch theory [14] overestimates the theoretical compressive strength compared with the continuum theory. Thus, the result (8) is closer to the experimental results, since all theoretical compressive strengths are as a rule higher than the corresponding experimental values.

2. For composites with small matrix concentration,

$$S_m \to 0, \qquad S_r \to 1, \tag{14}$$

the Dow–Gruntfest–Rosen–Schuerch theory produces a physically inconsistent result. For example, (12) with (14) yields

$$(\Pi_1^-)_{T[14]} \to \infty. \tag{15}$$

Contrastingly, the continuum theory produces a physically consistent result for a homogeneous material. For example, (8) with (14) yields

$$(\Pi_1^-)_T \to G_r. \tag{16}$$

3. The theoretical compressive strength (12) predicted by the Dow–Gruntfest–Rosen–Schuerch theory follows from the theoretical compressive strength (8) predicted by the continuum theory if

$$\frac{S_{\mathrm{r}}}{S_{\mathrm{m}}}\frac{E_{\mathrm{m}}}{E_{\mathrm{r}}}<<1, \qquad 1+\frac{S_{\mathrm{r}}}{S_{\mathrm{m}}}\frac{E_{\mathrm{m}}}{E_{\mathrm{r}}}\approx 1, \tag{17}$$

i.e., for reinforcement of high rigidity and matrix of high concentration.

The above qualitative analysis indicates the continuum theory is preferred over the Dow–Gruntfest–Rosen–Schuerch theory.

This concludes the analysis of the continuum compressive-failure theory for laminated nanocomposites.

2.1.2. Fibrous Nanocomposites. Continuum Approximation. According to Fig. 1, we are dealing with a spatial problem for fibrous unidirectional nanocomposites compressed along the Ox_3-axis. The CNTs are parallel and quite long and are modeled by infinite circular cylinders. Therefore, from (5) we obtain:

$$(\Pi_3^-)_T = \min\{\langle G_{31}\rangle, \langle G_{32}\rangle\}, \tag{18}$$

where $(\Pi_3^-)_T$ is the theoretical compressive strength measured along the Ox_3-axis and determined using the continuum compressive-failure theory for fibrous nanocomposites based on the TLTSDB, and $\langle G_{31}\rangle$ and $\langle G_{32}\rangle$ are the shear moduli determined using the homogeneous orthotropic linearly elastic model.

We will restrict ourselves to fibrous nanocomposites that do not have preferential reinforcement directions in the cross-sectional plane (x_3 = const), i.e., no regular structure provides orthotropy in the plane x_3 = const. In this case, a fibrous nanocomposite can be approximated by a transversely isotropic body with axis of isotropy coinciding with the Ox_3-axis (the plane x_3 = const is the plane of isotropy). For the indicated case from (18) we obtain the expression

$$(\Pi_3^-)_T = \langle G_{31}\rangle, \qquad \langle G_{31}\rangle = \langle G_{32}\rangle. \tag{19}$$

Expression (19) can be applied to relatively short CNTs only if $\langle G_{31}\rangle$ is known for a nanocomposite reinforced with such CNTs (cylinders of finite length).

In the case of infinitely long CNTs (modeled by infinite hollow circular cylinders), the quantity $\langle G_{31}\rangle$ can be determined from the expression in [1, p. 97]. Substituting this expression into (19), we obtain

$$(\Pi_3^-)_T = G_{\mathrm{m}}\frac{1+S_{\mathrm{r}}+S_{\mathrm{m}}\dfrac{G_{\mathrm{m}}}{G_{\mathrm{r}}}\dfrac{1+q^2}{1-q^2}}{S_{\mathrm{m}}+(1+S_{\mathrm{r}})\dfrac{G_{\mathrm{m}}}{G_{\mathrm{r}}}\dfrac{1+q^2}{1-q^2}}, \tag{20}$$

where G_{r} and G_{m} are the shear moduli of the reinforcement (CNTs) and matrix; S_{r} and S_{m} are the volume concentrations of the CNTs and matrix; $q = r_2 r_1^{-1}$, and r_2 and r_1 are the inner and outer radii of the hollow CNT.

If (4), then (20) reduces to

$$(\Pi_3^-)_T = G_{\mathrm{m}}\frac{1+S_{\mathrm{r}}+S_{\mathrm{m}}\dfrac{E_{\mathrm{m}}}{E_{\mathrm{r}}}\dfrac{1+q^2}{1-q^2}}{S_{\mathrm{m}}+(1+S_{\mathrm{r}})\dfrac{E_{\mathrm{m}}}{E_{\mathrm{r}}}\dfrac{1+q^2}{1-q^2}}. \tag{21}$$

Expression (21) applies to CNTs with different wall thicknesses that can be modeled by hollow and solid cylinders. Setting $q = 0$ in (21), we obtain an expression for the theoretical compressive strength of a fibrous nanocomposite with CNTs modeled by solid cylinders:

$$(\Pi_3^-)_T = G_{\mathrm{m}}\frac{1+S_{\mathrm{r}}+S_{\mathrm{m}}\dfrac{E_{\mathrm{m}}}{E_{\mathrm{r}}}}{S_{\mathrm{m}}+(1+S_{\mathrm{r}})\dfrac{E_{\mathrm{m}}}{E_{\mathrm{r}}}}. \tag{22}$$

TABLE 5

h, nm	CNT	D, nm						
		4	5	10	15	20	25	30
0.35	single-layer	0.167	0.134	0.067	0.045	0.034	0.027	0.022
0.670	two-layer	0.335	0.268	0.134	0.089	0.067	0.054	0.044
1.005	three-layer	0.502	0.402	0.201	0.134	0.100	0.080	0.067
1.340	four-layer	0.670	0.530	0.268	0.179	0.134	0.107	0.089

Expression (22) coincides with expression (2.66) in [7, p. 96] in view of (4).

For thin-walled CNTs, expression (21) can be simplified by adopting the approximation

$$1+hr_1^{-1} \approx 1, \qquad hr_1^{-1} << 1, \tag{23}$$

where r_1 and h are the outer radius and wall thickness of the hollow CNT. In view of (23), expression (21) reduces to

$$(\Pi_3^-)_T = G_m \frac{1+S_r+S_m \dfrac{D}{2h}\dfrac{E_m}{E_r}}{S_m+(1+S_r)\dfrac{D}{2h}\dfrac{E_m}{E_r}}, \tag{24}$$

where D is the CNT diameter. Table 5 collects the values of the parameter $hr_1^{-1} = 2hD^{-1}$ appearing in (22) for different values of D and h, according to the data presented in Sect. 1.1. From Table 5, it follows that there are CNT that meet the second condition in (23) and allow expression (24) to be used. In most cases, it is appropriate to apply expression (21).

Expression (20) can be rearranged as

$$(\Pi_3^-)_T = \frac{G_m}{S_r} \frac{1+S_r+S_m \dfrac{E_m}{E_r}\dfrac{1+q^2}{1-q^2}}{1+\dfrac{1+S_r}{S_m}\dfrac{E_m}{E_r}\dfrac{1+q^2}{1-q^2}}. \tag{25}$$

Comparing (12) and (25) reveals that the theoretical compressive strength (12) predicted by the Dow–Gruntfest–Rosen–Schuerch theory does not follow from that (25) for fibrous nanocomposites under any conditions, including conditions (17). This conclusion appears to follow from the fact that fibers in a fibrous nanocomposite interact in a more involved manner than in a laminated nanocomposite. Therefore, a plane analysis of the failure mechanism for laminated nanocomposites cannot describe all specific features of the failure mechanism for fibrous nanocomposites, which was indicated in Introduction. It is worth repeating here that the fundamental results [14] in the Dow–Gruntfest–Rosen–Schuerch theory have been obtained within the framework of a plane problem for laminated composites.

As with laminated nanocomposites (Sect. 2.1.1), expressions (21), (22), (24), and (25) for fibrous nanocomposites (Fig. 1) enable us to determine the limit strain $\langle \varepsilon_{33}^0 \rangle$ along the Ox_3-axis at failure due to microbuckling. According to Fig. 1, the subcritical deformation of fibrous nanocomposites is described by

$$\langle \varepsilon_{33}^0 \rangle = \varepsilon_{33}^{0r} = \varepsilon_{33}^{0m} = \langle \varepsilon_{fr} \rangle, \tag{26}$$

where $\langle \varepsilon_{33}^0 \rangle$ is the microbuckling strain measured along the Ox_3-axis; ε_{33}^{0r} and ε_{33}^{0m} are the corresponding microbuckling strains of the reinforcement and matrix along the Ox_3-axis; and $\langle \varepsilon_{fr} \rangle$ is the failure strain.

TABLE 6

S_r, %	5	10	15	20	25	30	40	50
$\langle \varepsilon_{fr} \rangle$, %	2.52	1.54	1.12	0.94	0.83	0.77	0.73	0.71

Young's modulus $\langle E_3 \rangle$ can easily be determined from the equilibrium condition using the homogeneous orthotropic model with effective constants:

$$\langle E_3 \rangle = S_r E_r + S_m E_m . \tag{27}$$

Expression (27), as well as (10), has been derived using one-dimensional models for the matrix and reinforcement, since by virtue of (4), transverse effects in nanocomposites are accounted for approximately. The scientific literature associates expressions (10) and (27) with mixture theory. In (27), as in (10), E_r and E_m are Young's moduli of the reinforcement and matrices. Since transverse effects in nanocomposites are accounted for approximately here, we will use a one-dimensional model to estimate $\langle \varepsilon_{fr} \rangle$. Thus, (21) and (27) yield

$$\langle \varepsilon_{fr} \rangle = \frac{G_m}{E_r S_r S_m} \frac{1}{1+\dfrac{S_m}{S_r}\dfrac{E_m}{E_r}} \frac{1+S_r+S_m \dfrac{E_m}{E_r}\dfrac{1+q^2}{1-q^2}}{1+\dfrac{1+S_r}{S_m}\dfrac{E_m}{E_r}\dfrac{1+q^2}{1-q^2}} . \tag{28}$$

Expression (28) can be simplified in two special cases, by analogy with (22) and (23).

As an example, we will use expression (28) to calculate $\langle \varepsilon_{fr} \rangle$ for a three-layer CNT with h = 1.005 nm and D = 10 nm. According to Table 5, $hr_1^{-1} = 2hD^{-1} = 0.201$. Thus, the second condition in (23) is not satisfied, simplification (24) cannot be applied, and expression (28) should be used. Table 6 includes values of $\langle \varepsilon_{fr} \rangle$ for different reinforcement concentrations in fibrous nanocomposite. The reinforcement concentrations (S_r) are selected the same as in Table 4 for laminated composites, the mean Young's moduli (1) for CNT and (3) for polymeric matrix are used, and condition (4) is taken into account. Comparing Tables 4 and 6 shows that the limit strains in fibrous nanocomposites are somewhat larger than in laminated nanocomposites.

Let us compare the microbuckling strain $\langle \varepsilon_{fr} \rangle$ (determined using the linearly elastic model) for fibrous nanocomposite and the elastic limit strain ε_1^m for polymer matrix. Using the values of E_m and σ_1^m in Table 3 for different matrices, we obtain: ε_1^m = 1–2.1% (epoxy), ε_1^m = 1–1.5% (polyester), ε_1^m = 1–1.3% (phenolformaldehyde), ε_1^m = 1–0.9% (organic silicon), ε_1^m = 1.3% (epoxy phenolic-butyral), and ε_1^m = 2.4% (epoxy maleic). Note that the values of $\langle \varepsilon_{fr} \rangle$ for fibrous nanocomposite in Table 6 are equally valid for the matrix, by virtue of (26). Comparing the values of $\langle \varepsilon_{fr} \rangle$ from Table 6 and the above-mentioned values of ε_1^m for different matrices reveals that the linearly elastic model is applicable to a fibrous nanocomposite with $S_r \geq 20\%$ in studying microbuckling as a compressive-failure mechanism for nanocomposites. A similar conclusion has been formulated in Sect. 2.1.1 for laminated nanocomposites. Let us now formulate a general conclusion as to the compressive-failure theory for fibrous and laminated nanocomposites.

General Conclusion. In developing a compressive-failure theory for a wide range of nanocomposites, the linearly elastic model can be applied when the failure mechanism is microbuckling.

This conclusion pertains to the continuum-failure theory based on the TLTSDB.

This concludes the analysis of the continuum compressive-failure theory for fibrous composites.

2.1.3. Surface Failure. Continuum Approximation. Sections 2.1.1 and 2.1.2 addressed the continuum compressive-failure theory for laminated and fibrous nanocomposites in the case where failure extends throughout the entire material. Since the material is considered infinite, this type of failure is internal failure of the entire material or structural member. The theoretical compressive strengths for this type of failure are defined by (6)–(8) and (18)–(21). Along with this type

of failure, surface failure was addressed in [7]. Surface failure is a process that localizes near the boundary surfaces and diminishes with depth.

For a wide range of composites, it was strictly proved in [7] that the theoretical compressive strengths corresponding to surface failure are somewhat less than those defined by (6)–(8) and (18)–(21) and corresponding to internal failure. This conclusion is equally valid for laminated and fibrous nanocomposites.

Thus, the continuum compressive-failure theory under consideration suggests that the failure process goes as follows: Failure sets in under stresses that are slightly less than the theoretical compressive strengths (6)–(8) and (18)–(21) and localizes near the surface. After the stresses reach the levels (6) – (8) and (18) – (21), the failure extends avalanche-like throughout the entire material.

This concludes the analysis of the continuum compressive-failure theory based on the approach from [2, 7].

2.2. Piecewise-Homogeneous Model. Let us discuss the basic results obtained in developing the compressive-failure theory for fibrous unidirectional (Fig. 1) and laminated (Fig. 2) nanocomposites in the case where composites are modeled, according to [3], by a piecewise-homogeneous material, and the reinforcement (CNT) and polymeric matrix are described by the three-dimensional linear theory of stability of deformable bodies [4, 6, 19] with continuity conditions for the stress and displacement vectors satisfied at the reinforcement–matrix interface. As in the previous section, the subscripts "r" and "m" will refer to the matrix and reinforcement (CNT), respectively. We will assume that the acting loads are dead, which is sufficient [4, 6, 19] for the applicability of the static formulation. The reinforcement and matrix will be modeled by nonlinearly elastic materials. For specific nanocomposites, we will apply linearly elastic models, since, as proved in Sect. 2.1.2, they can be applied to a wide range of nanocomposites in developing a compressive-failure theory with microbuckling as a failure mechanism. Such an approach [3, 7] employs the general TLTSDB solutions [4, 6, 19]. This leads to the task of minimizing the roots of the characteristic equations with respect to the waveformation parameters of the corresponding buckling modes.

In the previous section, we have detailed all the aspects of the development of the continuum (approach [2]) compressive-failure theory for fibrous and laminated nanocomposites in the case where the failure mechanism is microbuckling. This approach has produced a significant result formulated in Sect. 2.1.2 as the general conclusion: The linearly elastic model can be applied to the reinforcement and matrix of a wide range of nanocomposites in studying the microbuckling phenomenon. In the current section, we will analyze the development of the compressive-failure theory for nanocomposites modeled by a piecewise-homogeneous body (approach [3]) based on the TLTSDB. We will restrict ourselves to just the basic aspects of theory development.

The compressive-failure theory under consideration is based on analyzing the microbuckling phenomenon. To apply the piecewise-homogeneous model [3], which will be used to determine the critical load and buckling mode, it is necessary to give a more clear definition to microbuckling (internal instability). According to [7], the internal instability of nanocomposites is microbuckling occurring at certain relationships between the stiffness characteristics and concentrations of the reinforcement and matrix, from which it is possible to determine the critical load and buckling mode, irrespective of the geometry of and boundary conditions for the structural member. Internal instability occurs in structural members made of nanocomposites when the critical load corresponding to microbuckling (internal instability) is less than the critical load corresponding to buckling of the structural member and the microbuckling wavelength is much less than the typical (minimum) length scale of the structural member. Let us introduce the following notation: p_{cr} is the critical load corresponding to internal instability; $p_{\mathrm{cr}}^{\mathrm{sm}}$ is the critical load corresponding to buckling of the structural member; L is the typical (minimum) length scale of the structural member; and l_{cr} is the microbuckling half-wavelength. Thus, microbuckling occurs when

$$p_{\mathrm{cr}} < p_{\mathrm{cr}}^{\mathrm{sm}}, \qquad l_{\mathrm{cr}} << L. \tag{29}$$

From the above discussion, it follows that internal instability occurs only when it is possible to determine the critical force and buckling mode for an infinite nanocomposite (no effect of geometry and boundary conditions). Let p be the load parameter, α be the waveformation parameter of the buckling mode, l be the buckling half-wavelength, and h be the typical (minimum) length scale (which may be either the thickness of the reinforcement layer h_{r} or the thickness of the matrix layer h_{m} in the case of laminated nanocomposites). The parameters p and α are defined by

$$p = (-\sigma_{11}^{0\mathrm{r}})E_{\mathrm{r}}^{-1}, \qquad \alpha = \pi \frac{h}{l}. \tag{30}$$

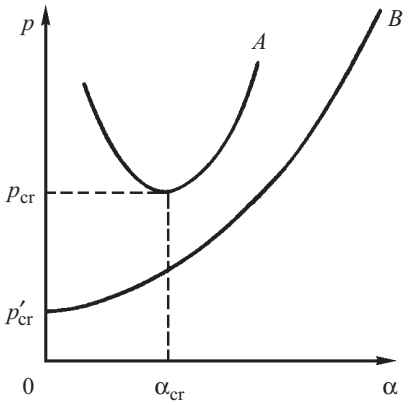

Fig. 7

Solving the corresponding characteristic equations based on the piecewise-homogeneous model, we obtain

$$p = p(\alpha). \tag{31}$$

Two types of dependences (31) are shown in Fig. 7 for illustration (curves *A* and *B*).

The curve *A* has a well-defined minimum; therefore, p_{cr} is determined by minimizing (31) with respect to α, resulting in the expression $p_{cr} = p(\alpha_{cr})$. Hence, in the case of curve *A*, we can determine p_{cr} and the buckling mode corresponding to $\alpha_{cr} = \pi h l_{cr}^{-1}$. Note that for the curve *A* the following conditions are satisfied:

$$\alpha_{cr} \neq 0, \quad l_{cr} \neq \infty. \tag{32}$$

The curve *B* is monotonic; therefore, p_{cr} is determined by minimizing (31) with respect to α, resulting in the expression $p_{cr} = p(0)$. Thus, for the curve *B*, it follows from (30) that

$$\alpha_{cr} = 0, \quad l_{cr} = \infty. \tag{33}$$

From the second expression in (33) it follows that the second condition in (29) is not satisfied for any finite structural member. Thus, internal instability does not occur in the case of curve *B*. What this means is that for each specific nanocomposite modeled by a piecewise-homogeneous material, it is necessary to prove that internal instability (microbuckling) can occur, leading to failure under compression.

This concludes the discussion of fibrous and laminated nanocomposites modeled by piecewise-homogeneous material. Now we will briefly analyze the basic aspects separately for laminated and fibrous nanocomposites.

2.2.1. Laminated Nanocomposites. Piecewise-Homogeneous Model. According to Fig. 2, we are dealing with a two-dimensional problem (plane x_1Ox_2) for a laminated nanocomposite with layers of reinforcement and matrix alternating along the Ox_2-axis and a load acting along the Ox_1-axis, according to conditions (9). The three-dimensional problem [7] where layers of reinforcement and matrix alternate along one axis is treated similarly. Lacking space, we will discuss the formulations and solutions for the plane problem represented in Fig. 2 (see [7] for a complete analysis of the three-dimensional problem). Note that the results reported in [7] pertain to a wide range of laminated composites (whose relative stiffness and geometry vary over wide ranges). These results are equally valid for laminated nanocomposites, in view of the mechanical properties and geometry of CNT-reinforcement and polymer matrix, outlined in the first section. Thus, we will briefly analyze the results for laminated composites obtained in [7] using the piecewise-homogeneous model (approach [3]) and the TLTSDB [4, 6, 19].

As already mentioned, laminated nanocomposites are periodic in the direction perpendicular to the layers (along the Ox_2-axis). In this connection, the solutions of the basic TLTSDB equations have the form of functions periodic along the Ox_2-axis (Fig. 2) with a period multiple of the structural period. Following [7], we will use the following quantities to characterize the buckling modes along the Ox_2-axis: $2h_r$ and $2h_m$, the thicknesses of the reinforcement and matrix layers; and u_2^r and u_2^m, the displacements along the Ox_2-axis in the layers of reinforcement and matrix. We will consider four different buckling modes shown in Fig. 8*a*, *b*, *c*, *d.*

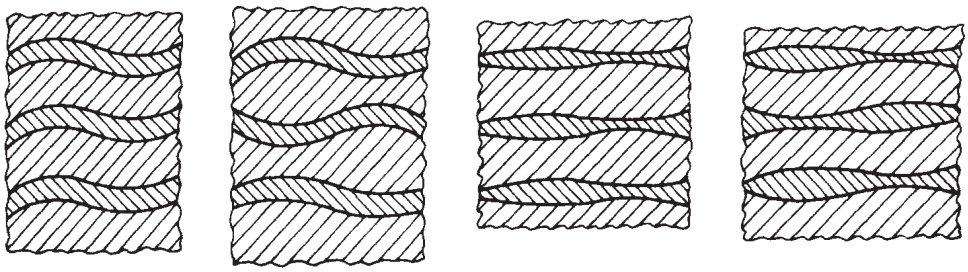

a *b* *c* *d*

Fig. 8

The buckling mode of the first kind (Fig. 8*a*) has a period equal to the structural period, $2(h_r + h_m)$. The corresponding displacements u_2^r and u_2^m are symmetric about the median surface of each layer. This buckling mode may be called flexural or antisymmetric, due to the nature of deformation of reinforcement and matrix (in [14] it is called a shear mode).

The buckling mode of the second kind (Fig. 8*b*) has a period equal to the doubled structural period, $4(h_r + h_m)$. The corresponding displacements u_2^m and u_2^r are antisymmetric and symmetric, respectively, about the median surface of each layer. This buckling mode is called in [14] a tensile mode.

The buckling mode of the third kind (Fig. 8*c*) has a period equal to the structural period, $2(h_r + h_m)$. The corresponding displacements u_2^r and u_2^m are antisymmetric about the median surface of each layer. This buckling mode may be called a tensile mode.

The buckling mode of the fourth kind (Fig. 8*d*) has a period equal to the doubled structural period, $4(h_r + h_m)$. The displacements u_2^r and u_2^m are antisymmetric and symmetric, respectively, about the median surface of each layer.

The above buckling modes exhaust all possible modes with periods equal to either the structural period or the doubled structural period. Buckling modes with higher period

$$T = 2k(h_r + h_m), \quad k = 3, 4, \ldots, \tag{34}$$

can be treated similarly.

Buckling modes of the first to fourth kinds were described in [7] for a wide range of laminated composites using the approach from [3] based on the piecewise-homogeneous model and TLTSDB. Note that the Dow–Gruntfest–Rosen–Schuerch theory predicted only buckling modes of the first and second kinds.

As already repeatedly mentioned, the failure theory for nanocomposites based on the piecewise-homogeneous model and TLTSDB is the most exact and rigorous in solid mechanics and, naturally, can be used to estimate other approximate theories. Since the compressive-failure theory for laminated nanocomposites has been developed using the above-mentioned approach, it can be used to estimate the continuum failure theory described in Sect. 2.1.1 and the Dow–Gruntfest–Rosen–Schuerch theory. In this connection, we will look at asymptotically exact approximate compressive-failure theories for nanocomposites [7].

An approximate theory is called asymptotically exact if for

$$\alpha = \pi \frac{h_r + h_m}{l} \to 0, \quad \text{i.e.,} \quad l \to \infty, \tag{35}$$

this theory follows from the corresponding rigorous theory based on the piecewise-homogeneous model and TLTSDB. In the theory of elastic waves, conditions (35) define the long-wave approximation. In [7] it was strictly proved that the continuum compressive-failure theory for laminated composites (see Sect. 2.1.1) is asymptotically exact and follows from the theory being considered when condition (35) is satisfied for the buckling mode of the first kind (Fig. 8*a*). This result has been obtained for a wide range of laminated composites, including laminated nanocomposites with parameters (1) and (3). As already mentioned in Sect. 2.1.1, the Dow–Gruntfest–Rosen–Schuerch theory is different from the continuum compressive-failure theory for nanocomposites. Thus, the Dow–Gruntfest–Rosen–Schuerch theory is not asymptotically exact.

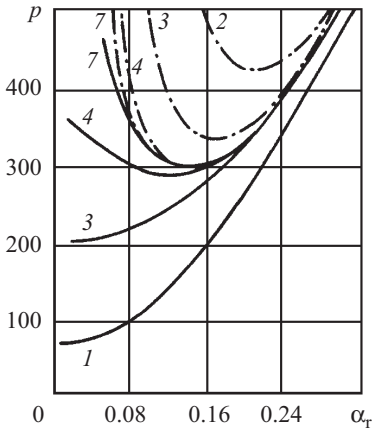

Fig. 9

Let us now discuss a number of specific numerical results from the compressive-failure theory for laminated nanocomposites with parameters (1) and (3). From (1) and (3) it follows that

$$E_r E_m^{-1} = 300. \tag{36}$$

Let

$$p = -\langle \varepsilon_{11}^0 \rangle \frac{1}{1-\nu} \cdot 10^4 = -\frac{\sigma_{11}^{0r}}{E_r}(1+\nu) \cdot 10^4, \quad \alpha_r = \pi \frac{h_r}{l}, \quad \langle \varepsilon_{11}^0 \rangle = \varepsilon_{11}^{0r} = \varepsilon_{11}^{0m}. \tag{37}$$

Solving the corresponding characteristic equations, we obtain the dependence $p = p(\alpha_r)$ for the following geometrical parameters:

$$h_m h_r^{-1} = 1, 5, 10, 20, 30, 40, 50. \tag{38}$$

Figure 9 shows the dependences $p(\alpha_r)$ for values (36) and (38) (curves *1–7*) and for $\nu = 0.3$ because Poisson's ratio for a series of polymeric matrices (Table 3) is close to 0.3. The solid lines in Fig. 9 represent the buckling mode of the first kind (Fig. 8*a*) and the dashed lines, the buckling mode of the second kind (Fig. 8*b*). An analysis of Fig. 9 leads us to the following conclusions.

1. The buckling mode of the first kind (Fig. 8*a*) does not occur for all concentrations of CNT and matrix, since some solid curves in Fig. 9 are monotonic (curves *1* and *3*), as the curve *B* in Fig. 7.

2. The buckling mode of the second kind (Fig. 8*b*) may occur for all values of parameters (38), since all the dash-and-dot curves in Fig. 9 have a minimum (curves *2–4* and 7 in Fig. 9), as the curve *A* in Fig. 7.

3. When the buckling modes of the first and second kinds may occur, there are some concentrations of CNT and matrix for which the failure loads corresponding to these modes differ insignificantly. For example, the minimums of solid and dash-and-dot curves *7* in Fig. 9 coincide (the failure loads and waveformation parameters are equal).

The results in Fig. 9 were borrowed from [7, p. 180].

The above qualitative and quantitative conclusions follow neither from the continuum theory (Sect. 2.1.1), though it is based on the TLTSDB, nor from the Dow–Gruntfest–Rosen–Schuerch theory.

Let us compare results for laminated nanocomposites produced by the exact failure theory being considered and by the continuum theory (Sect. 2.1.1). Table 7 collects values of the theoretical compressive strength ($(\Pi_1^-)_T$) for (4), (36), some of (38), and $v_r = v_m = 0.3$. The first row includes the results obtained using the piecewise-homogeneous model and TLTSDB, and the second row includes the results obtained using the continuum failure theory and TLTSDB. Table 7 was borrowed from [7, p. 197].

An analysis of Table 7 reveals that the continuum theory (Sect. 2.1.1) overestimates the theoretical compressive strength for laminated nanocomposites, compared with the piecewise-homogeneous model (Sect. 2.2.1). Since the estimate (13)

TABLE 7

$(\Pi_1^-)_T E_r^{-1} \cdot 10^4$	$h_m h_r^{-1}$			
	20	30	40	50
Piecewise-homogeneous model	10.5	7.9	6.2	4.4
Continuum theory	13.5	13.2	13.1	13.4

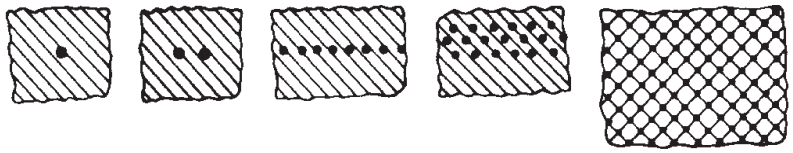

a *b* *c* *d* *e*

Fig. 10

always holds, the Dow–Gruntfest–Rosen–Schuerch theory even more overestimates the theoretical compressive strength, compared with the continuum failure theory (Sect. 2.1.1).

This concludes the discussion of the compressive-failure theory for laminated nanocomposites based on the piecewise-homogeneous model and TLTSDB.

2.2.2. Fibrous Nanocomposites. Piecewise-Homogeneous Model. According to Fig. 1, we are dealing with a three-dimensional problem for a fibrous unidirectional nanocomposite with infinite matrix and CNT reinforcement. The CNTs are modeled by infinite fibers of circular cross section aligned along the Ox_3-axis. It is assumed that prior to failure the reinforcement and matrix are loaded along the Ox_3-axis, resulting in identical contraction along the same axis, i.e., condition (26) is satisfied. Since the failure mechanism is microbuckling, all the considerations concerning this phenomenon (see Introduction) fit here. We will use the piecewise-homogeneous model [3, 7] and the TLTSDB [4, 6, 9]. Lacking space, we will analyze just the basic aspects of developing the failure theory for unidirectional fibrous nanocomposites.

Unidirectional fibrous nanocomposites compressed along the Ox_3-axis give rise to a great variety of problems associated with the variety of composite microstructures. Let us briefly analyze problems associated with the nanocomposite structure in the cross-sectional plane x_3 = const and schematically shown in Fig. 10*a*, *b*, *c*, *d*, *e.*

Figure 10*a* shows a fiber in an infinite matrix, which represents a fibrous nanocomposite with rather small concentration of CNTs. Here, the interaction of neighboring fibers during buckling can be neglected.

Figure 10*b* shows two fibers in an infinite matrix, which represents a fibrous composite with small concentration of CNTs and disordered (nonregular) structure in the cross-sectional plane (x_3 = const). Here, the interaction of neighboring fibers needs to be taken into account.

Figure 10*c* shows a periodic infinite row of fibers in an infinite matrix, which represents a fibrous nanocomposite with regular structure and considerable concentration of CNTs. Here, the interaction of fibers within a row should be taken into account.

Figure 10*d* shows several periodic infinite rows of fibers in an infinite matrix, which represents a fibrous nanocomposite with regular structure and considerable concentration of CNTs. Here, the interaction of fibers within one infinite periodic row and the interaction of fibers in several neighboring periodic rows should be taken into account.

Figure 10*e* shows a doubly periodic system of fibers in an infinite matrix, which represents a fibrous nanocomposite with regular structure and considerable concentration of CNTs. Here, the interaction of fibers within one infinite periodic row and the interaction of fibers between infinite rows should be taken into account.

Nanocomposites of stochastic structure could also be considered. The model of stochastic structure turned out to be promising in determining the effective characteristics of composites. An even greater variety of problems are associated with

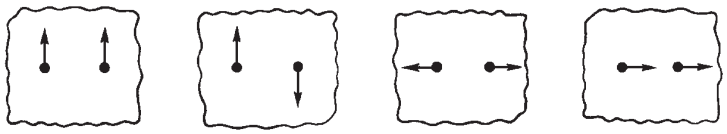

a *b* *c* *d*

Fig. 11

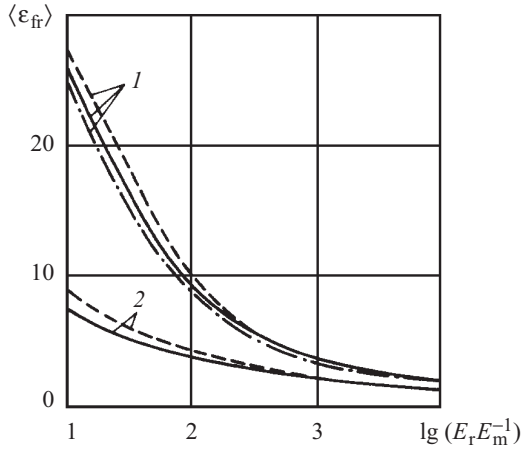

Fig. 12

buckling modes both along the CNT-axis (Ox_3-axis) and in the cross-sectional plane (x_3 = const). As an example, let us consider cross-sectional buckling modes (only in symmetry planes) for two fibers (Fig. 10*b*).

An out-of-plane in-phase buckling mode for two fibers is shown in Fig. 11*a*, an out-of-plane antiphase buckling mode for two fibers in Fig. 11*b*, an in-plane antiphase buckling mode for two fibers in Fig. 11*c*, and an in-plane in-phase buckling mode of two fibers in Fig. 11*d*. Physical considerations suggest that the minimum critical load corresponds to out-of-plane buckling if the plane of two fibers (horizontal plane in Fig. 11) is the plane of maximum stiffness. Similar conclusions can be drawn for the other structures in Fig. 10 and the like. Thus, to determine the critical load, it is necessary to minimize the load parameter with respect to both the buckling wavelength along the Ox_3-axis and buckling modes such as those in Fig. 11*a*, *b*, *c*, *d*.

Remark. Since CNTs are expediently modeled by hollow cylindrical fibers, for some relatively thin CNTs (Table 5) it is quite natural to analyze shell buckling modes, using applied two-dimensional theories of stability of thin-walled shells. Two considerations are important here: (i) the TLTSDB describes shell buckling modes as a partial case and (ii) though CNT-fibers are described by applied two-dimensional theories of stability of thin-walled shells, the matrix should be described by the TLTSDB, since it is the stability of the whole nanocomposite that is analyzed (Fig. 1). These considerations equally apply to the approach from [31].

Let us look at methods of solving failure problems for fibrous nanocomposites (Fig. 1) using piecewise-homogeneous models and the TLTSDB. As indicated in Sect. 2, the compressive-failure theory for nanocomposites is based on the assumption (4) that Poisson's ratios of the reinforcement and matrix are equal. Let us examine the influence of condition (4) on the solution of the failure problem for one fiber in an infinite matrix (Fig. 10*a*). Let the waveformation parameter along the Ox_3-axis (Fig. 1) be defined by

$$\alpha = \pi \frac{R}{l}, \qquad \alpha_{\rm cr} = \pi \frac{R}{l_{\rm cr}}, \tag{39}$$

where R is the fiber radius, and l is the buckling half-wavelength along the Ox_3-axis. Figure 12 shows the dependences of $\langle \varepsilon_{\rm fr} \rangle$ (26) and of $\alpha_{\rm cr}$ (39) on the parameter $\lg (E_{\rm r} E_{\rm m}^{-1})$ (curves *1* and *2*, respectively). The solid curves correspond to $\nu_{\rm r} = 0.2$ and $\nu_{\rm m} = 0.4$ (condition (4) is not satisfied), the dashed curves to $\nu_{\rm r} = \nu_{\rm m} = 0.2$ (condition (4) is satisfied), and the dash-and-dot curves to $\nu_{\rm r} = \nu_{\rm m} = 0.4$ (condition (4) is satisfied). Figure 12 is borrowed from [7, pp. 233, 234]. An analysis of Fig. 12 indicates [7] that the difference between Poisson's ratios of the reinforcement and matrix is less than 5% and may be neglected if

TABLE 8

$\langle \varepsilon_{fr} \rangle$, %	S_r, %						
	single fiber	4.1	11	15.3	21.2	24.8	32.8
Theory	5.0	3.15	2.06	1.89	1.68	1.59	1.52
Experiment				2.3	1.7	1.6	1.3

$$E_r E_m^{-1} \geq 20. \tag{40}$$

Since $E_r E_m^{-1}$ is defined by (36) for nanocomposites, condition (40) is automatically satisfied. Thus, we have proved that condition (4) applies to nanocomposites. This conclusion pertains only to nanocomposites with rather small concentration of CNTs (Fig. 10*a*) and can be extended to the other cases (Fig. 10*b*, *c*, *d*, *e*) only approximately.

Thus, after justification and application of condition (4), the general method of solving compressive-failure problems represented in Fig. 1 and 10*a*, *b*, *c*, *d*, *e* for fibrous nanocomposites modeled by a piecewise-homogeneous material includes the following stages:

1. Applying the general TLTSDB solutions [4, 6, 19] for homogeneous subcritical states.

2. Expanding the solutions of the governing equations for the reinforcement and matrices into Fourier series in trigonometric and cylindrical functions in each local coordinate system.

3. Applying the summation theorems for cylindrical functions to obtain solutions in the form of series with separated variables in each local coordinate system.

4. Satisfying the boundary conditions on local interfaces and inside surface of cylindrical CNTs in each local coordinate system.

5. Deriving characteristic equations in the form of infinite determinants.

6. Proving that these infinite determinants are of normal type. This proof justifies the replacement of infinite determinants by finite determinants of high order.

7. Calculating and analyzing critical loads.

This method allows solving a wide range of compressive-failure problems for fibrous nanocomposites that have cross-sectional structures (in the plane x_3 = const in Fig. 1) shown in Fig. 10*a*, *b*, *c*, *d*, *e.* It is significant that, according to Table 5, the method considers hollow fibers, which are CNTs modeled by circular cylinders, as contrasted to [7] where fibrous composites with solid fibers are studied.

In summary, it should be noted that the structures in Fig. 10*a*, *b*, *c*, *d* represent just model problems of the mechanics of fibrous composites, including fibrous nanocomposites. Fibrous composites have a doubly periodic structure, as in Fig. 10*e*. It is this structure that should be theoretically analyzed against experimental data. As an illustration, let us examine a fibrous composite with stainless steel wire reinforcement and aluminum matrix. Such a composite was studied in [7, Ch. 4] using an elastoplastic model for the matrix. Table 8 summarizes the failure strains $\langle \varepsilon_{fr} \rangle$ for one fiber (Fig. 10*a*) and for a fibrous composite with different reinforcement concentration S_r (Fig. 10*e*). This table was borrowed from [7, pp. 242, 317]. An analysis of Table 8 reveals that the failure strain for a doubly periodic system of fibers is severalfold less than for one fiber ($\langle \varepsilon_{fr} \rangle = 5\%$). For example, $\langle \varepsilon_{fr} \rangle = 1.52\%$ for $S_r = 32.8\%$. Note that the experimental data in Table 8 admit no different interpretations (see [7] for a detailed discussion). The indicated tendency (severalfold decrease in $\langle \varepsilon_{fr} \rangle$ upon passage from one fiber to a fibrous composite with doubly periodic structure) should also be observed for nanocomposites. For example, from Fig. 12 for one fiber and in view of (36) we obtain $\langle \varepsilon_{fr} \rangle \approx 6\%$ for nanocomposite, which corresponds to the case of one fiber in Table 8.

This concludes the discussion of developing the compressive-failure theory for fibrous nanocomposites based on the piecewise-homogeneous model and TLTSDB.

2.2.3. Surface Failure. Piecewise-Homogeneous Model. Sections 2.2.1 and 2.2.2 addressed the compressive-failure theory for laminated and fibrous nanocomposites in the case where failure extends throughout the entire material. Since the material is considered infinite, this type of failure can be called internal failure when the piecewise-homogeneous model is used.

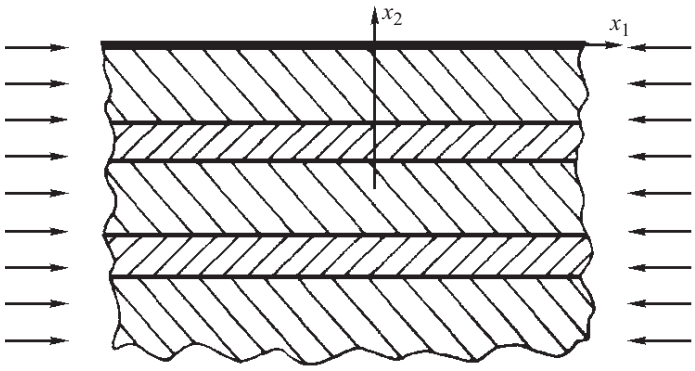

Fig. 13

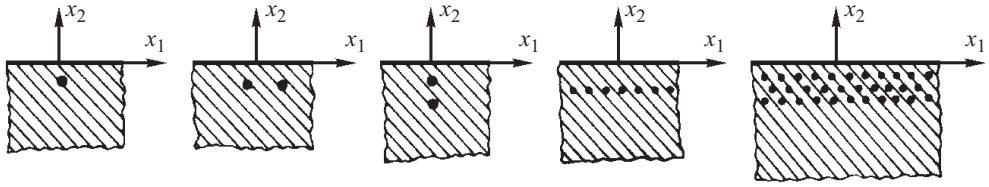

a *b* *c* *d* *e*

Fig. 14

As with the continuum theory (Sect. 2.1.3), the piecewise-homogeneous model allows studying the surface or near-surface failure of laminated and fibrous nanocomposites. Surface failure is compressive failure that localizes near the boundary surfaces and diminishes with depth from the surface. Phenomena of surface failure in laminated and fibrous nanocomposites studied within the framework of the piecewise-homogeneous model require surface and attenuation conditions to be satisfied, in addition to periodicity and continuity conditions for the stress and displacement vectors (Sects. 2.2.1 and 2.2.2).

Figure 13 shows a design model for analysis of the (near-)surface failure (in the plane x_1Ox_2) of a laminated nanocomposite compressed along the Ox_1-axis (the matrix and reinforcement contract equally along the Ox_1-axis). In this case, boundary conditions on the surface $x_2 = 0$ (Fig. 13) and attenuation conditions as $x_2 \to -\infty$ should be satisfied.

A richer variety of problems arises in studying the near-surface compressive failure of fibrous nanocomposites using the piecewise-homogeneous model. Let us briefly consider some aspects of such problems for nanocomposites having the surface $x_2 = 0$ and axially compressed along the Ox_3-axis. We will restrict ourselves to the case of failure problems for the plane $x_3 = \text{const}$. Different problems for fibrous nanocomposites are represented in Fig. 14*a*, *b*, *c*, *d*, *e.*

Figure 14*a* shows one fiber in a semi-infinite matrix, which represents a fibrous nanocomposite with rather small concentration of CNTs. Here, the interaction of neighboring fibers may be neglected.

Figure 14*b* shows two fibers in a semi-infinite matrix with centers of cross sections located on the free surface; and Fig. 14*c* shows two fibers in a semi-infinite matrix with centers of cross sections located on a line perpendicular to the free surface. The figures represent fibrous nanocomposites with small concentration of CNTs and disordered (nonregular) structure in the cross-sectional plane ($x_3 = \text{const}$). In the case of internal failure, the problems (Fig. 14*b*, *c*) go over into one problem (Fig. 10*b*).

Figures 14*d* and 14*e* show one row of fibers and several rows of fibers, their cross-section centers located on the boundary surface. The list of near-surface failure problems for fibrous nanocomposites is incomplete.

Mathematical methods for solving problems formulated above are described in [7].

Conclusions. Thus, we have outlined the fundamentals of the compressive-failure theory for laminated and fibrous nanocomposites with polymer matrix in the case where failure begins with microbuckling.

The basic results (problem formulations, solution methods, specific results and their analysis) have been obtained using the following two approaches (models). The first approach (continuum failure theory) employs the homogeneous anisotropic model with effective constants (homogenized material). In this case, the microstructural parameters appear in the expressions for the effective constants of the homogeneous anisotropic body. The second approach uses the piecewise-homogeneous model and,

separately for the reinforcement and matrix, the three-dimensional theory. In this case, continuity conditions for the stress and displacement vectors should be satisfied at the reinforcement–matrix interface.

A typical feature of the results is the application (in both approaches) of the three-dimensional linear theory of stability of deformable bodies [4, 6, 19]. Thus, the results expounded here may be considered exact and strict. That is why the results do not include errors inherent in the one- and two-dimensional applied theories of stability of rods, plates, and shells.

The results outlined here can be used to solve a wide range of problems for laminated and fibrous nanocomposites with different microstructures. Results of such studies could be reported in separate publications.

The authors express sincere gratitude to colleagues from the Center for Micro- and Nanomechanics at the University of Aberdeen, Scotland, for the help in preparing the paper.

REFERENCES

1. G. A. Van Fo Fy, *Theory of Reinforced Materials* [in Russian], Naukova Dumka, Kiev (1971).
2. A. N. Guz, "Determination of theoretical ultimate compressive strength for reinforced materials," *Dokl. AN USSR*, *Ser. A*, No. 3, 236–238 (1969).
3. A. N. Guz, "Developing a stability theory for unidirectional fibrous materials," *Prikl. Mekh*., **5**, No. 2, 62–70 (1969).
4. A. N. Guz, *Stability of Three-Dimensional Deformable Bodies* [in Russian], Naukova Dumka, Kiev (1971).
5. A. N. Guz, "Brittle fracture criteria for compressed materials with imperfections," *Dokl. AN SSSR*, **285**, No. 4, 828–831 (1985**)**.
6. A. N. Guz, *Fundamentals of the Three-Dimensional Theory of Stability of Deformable Bodies* [in Russian], Vyshcha Shkola, Kiev (1986).
7. A. N. Guz, *Fracture Mechanics of Compressed Composites* [in Russian], Naukova Dumka, Kiev (1990).
8. A. N. Guz, "Description and study of some nonclassical problems of fracture mechanics and related mechanisms," *Int. Appl. Mech*., **36**, No. 12, 1537–1564 (2000).
9. I. A. Guz, "Stability of a composite compressed along an interfacial crack," *Dokl. AN SSSR*, **325**, No. 3, 455–458 (1992).
10. I. A. Guz, "Stability of a composite compressed along two interfacial macrocracks," *Dokl. AN SSSR*, **328**, No. 4, 437–439 (1993).
11. I. A. Guz, "Investigation of the stability of a composite in compression along two parallel structural cracks at the layer interfaces," *Int. Appl. Mech*., **30**, No. 11, 841–847 (1994).
12. I. A. Guz, "Problems of the stability of composite materials in compression along interlaminar cracks: Periodic system of parallel macrocracks," *Int. Appl. Mech*., **31**, No. 7, 551–557 (1995).
13. H. Liebowitz (ed.), *Fracture: An Advanced Treatise*, Vols. 1–7, Acad. Press, New York–London (1968–1972).
14. B. W. Rosen, "Mechanics of composite strengthening," in: *Fiber Composite Materials*, American Society of Metals, Metals Park, Ohio (1965), pp. 37–75.
15. G. P. Cherepanov, *Fracture Mechanics of Composite Materials* [in Russian], Nauka, Moscow (1983).
16. C. F. Cornwell and L. T. Wille, "Elastic properties of single-walled carbon nanotubes in compression," *Solid State Commun*., **101**, 555–558 (1997).
17. N. F. Dow and I. J. Gruntfest, "Determination of most needed potentially possible improvements in materials for ballistic and space vehicles," *General Electric Co.*, *Space Sci. Lab*., TISR 60 SD 389, June (1960).
18. C. Goze, L. Vaccarini, L. Henrard, P. Bernier, E. Hernandez, and A. Rubio, "Elastic and mechanical properties of carbon nanotubes," *Synth. Met*., **103**, 2500–2501 (1999).
19. A. N. Guz, *Fundamentals of the Three-Dimensional Theory of Stability of Deformable Bodies*, Springer-Verlag, Berlin–Heidelberg–New York (1999).
20. A. N. Guz, "On one two-level model in the mesomechanics of compression fracture of cracked composites," *Int. Appl. Mech*., **39**, No, 3, 274–285 (2003).
21. A. N. Guz and I. A. Guz, "Analytical solution of stability problem for two composite half-planes compressed along interfacial cracks," *Composites*, *Part B*, **31**, No. 5, 403–418 (2000).
22. A. N. Guz and I. A. Guz, "Mixed plane problems of linearized mechanics of solids: Exact solutions," *Int. Appl. Mech*., **40**, No. 1, 1–29 (2004).

23. A. N. Guz and J. J. Rushchitsky, "Nanomaterials: On mechanics of nanomaterials," *Int. Appl. Mech*., **39**, No. 11, 1264–1298 (2003).
24. I. A. Guz, "Computer-aided investigations of composites with various interlaminar cracks," *ZAMM*, **76**, Suppl. No. 5, 189–190 (1996).
25. T. Halicioglu, "Stress calculations for carbon nanotubes," *Thin Solid Films*, **312**, 11–14 (1998).
26. E. Hermandez, C. Goze, P. Bernier, and A. Rubio, "Elastic properties of C and $B_xC_yN_z$ composite nanotubes," *Phys. Rev. Lett*., **80**, 4502–4505 (1998).
27. E. Hermandez, C. Goze, P. Bernier, and A. Rubio, "Elastic properties of single-wall nanotubes," *Appl. Phys*., **A68**, 287–292 (1999).
28. A. Krishnan, E. Dujardin, T. W. Ebbesen, P. N. Yianilos, and M. M. J. Treacy, "Young's modulus of single-walled nanotubes," *Phys. Rev*., **B58**, 14013–14019 (1998).
29. G. V. Lier, C. V. Alsenoy, V. V. Doran, and P. Geerlings, "Ab initio study of the elastic properties of single-walled carbon nanotubes and graphene," *Chem. Phys. Lett*., **326**, 181–185 (2000).
30. K. M. Liew, X. Q. He, and C. H. Wong, "On the study of elastic and plastic properties of multi-walled carbon nanotubes under axial tension using molecular dynamics simulation," *Acta Mater*., **52**, 2521–2527 (2004).
31. O. Lourie, D. M. Cox, and H. D. Wagner, "Buckling and collapse of embedded carbon nanotubes," *Phys. Rev. Lett*., **81**, No. 8, 1638–1641 (1998).
32. O. Lourie and H. D. Wagner, "Evaluation of Young's modulus of carbon nanotubes by micro-Raman spectroscopy," *J. Mater. Res*., **13**, 2418–2422 (1998).
33. J. P. Lu, "Elastic properties of carbon nanotubes and nanoropes," *Phys. Rev. Lett*., **79**, 1297–1300 (1997).
34. J. M. Molina, S. S. Savinsky, and N. V. Khokhriakov, "A tight-binding model for calculation of structures and properties of graphitic nanotubes," *J. Chem. Phys*., **104**, 4652–4556 (1996).
35. J. Muster, M. Burghard, S. Roth, G. S. Duesberg, E. Hemander, and A. Rubio, "Scanning force microscopy characterization of individual carbon nanotubes on electrode arrays," *J. Vac. Sci. Technol*., **B16**, 2796–2801 (1998).
36. G. Overney, W. Zhong, and D. Tomanek, "Structural rigidity and low-frequency vibrational models of long carbon tubules," *Z. Phys.*, *D: Atoms Mol. Clusters*, **27**, 93–96 (1993).
37. Z. W. Pan, S. S. Xie, L. Lu, B. H. Chang, L. F. Sun, W. Y. Zhou, and G. Wang, "Tensile test of ropes of very long aligned multiwall carbon nanotubes," *Appl. Phys. Lett*., **74**, 3152–3154 (1999).
38. A. Pantano, D. M. Parks, and M. C. Boyce, "Mechanics of deformation of single- and multi-wall carbon nanotubes," *J. Mech. Phys. Solids*, **52**, 789–821 (2004).
39. V. N. Popov, V. E. Van Doren, and M. Balkanski, "Elastic properties of single-walled carbon nanotubes," *Phys. Rev*., **B61**, 3078–3084 (2000).
40. Y. I. Prylutskyy, S. S. Durov, O. V. Ogloblya, E. V. Buraneva, and P. Scharff, "Molecular dynamics simulations of mechanical, vibrational and electronic properties of carbon nanotubes," *Comput. Mater. Sci*., **17**, 352–355 (2000).
41. D. Qian, G. J. Wagner, W. K. Liu, M. F. Yu, and R. S. Ruoff, "Mechanics of carbon nanotubes," *Appl. Mech. Rev*., **55**, 495–530 (2002).
42. D. H. Robertson, D. W. Brenner, and J. W. Mintmire, "Energetics and nanoscale graphitic tubules," *Phys. Rev*., **B45**, 12592–12595 (1992).
43. J. P. Salventat, G. A. D. Briggs, J. M. Bonard, R. R. Bacsa, and A. J. Kulik, "Elastic and shear moduli of single-walled carbon nanotube ropes," *Phys. Rev. Lett*., **82**, 944–947 (1999).
44. D. Sanchez-Portal, E. Artacho, J. M. Soler, A. Rubio, and P. Ordejon, "Ab initio structural, elastic and vibrational properties of carbon nanotubes," *Phys. Rev*., **B59**, 12678–12688 (1999).
45. H. Schuerch, *Boron Filament Composite Materials for Space Structures*, *Pt. 1: Compressive Strength of Boron Metal Composite*, Rep. No. ARC-R-168, Astro Research Corp., Santa Barbara (Ca) (1964).
46. H. Schuerch, "Prediction of compressive strength in uniaxial Boron fibermetal composite materials," *AIAA J*., **4**, No. 1, 102–106 (1966).
47. D. Srivastava, Ch. Wei, and K. Cho, "Nanomechanics of carbon nanotubes and composites," *Appl. Mech. Rev*., **56**, 215–229 (2003).
48. T. W. Tombler, C. Zhou, L. Alezseyev, J. Kong, H. L. Dai, C. S. Jaganthi, M. Tang, and S. Y. Wu, "Reversible electromechanical characterictics of carbon nanotubes under local-probe manipulation," *Nature*, **405**, 769–772 (2000).

49. M. M. J. Treacy, T. W. Ebbesen, and J. M. Gibson, “Exceptionally high Young’s modulus observed for individual carbon nanotubes,” *Nature*, **381**, 678–680 (1996).
50. L. Vaccarini, C. Goze, L. Henrard, E. Hermandez, P. Bernier, and A. Rubio, “Mechanical and electronic properties of carbon and boron-nitride nanotubes,” *Carbon*, **38**, 1681–1690 (2000).
51. E. W. Wong, P. E. Sheehan, and C. M. Lieber, “Nanobeam mechanics: elasticity, strength and toughness of nanorods and nanotubes,” *Science*, **277**, 1971–1975 (1997).
52. B. L. Yakobson, C. J. Brabec, and J. Bernhole, “Nanomechanics of carbon tubes: instabilities beyond linear response,” *Phys. Rev. Lett*., **76**, 2511–2514 (1996).
53. M. F. Yu, O. Lourie, M. J. Dyer, K. Moloni, T. F. Kelly, and R. S. Ruoff, “Strength and breaking mechanism of multiwalled carbon nanotubes under tensile,” *Science*, **287**, 454–458 (2000).
54. P. Zhang, H. Jiang, Y. Huang, P. H. Geubelle, and K. C. Hwang, “An atomistic-based continuum theory for carbon nanotubes: analysis of fracture nucleation,” *J. Mech. Phys. Solids*, **52**, 977–998 (2004).
55. G. Zhou, W. Duan, and B. Gu, “First-principles study on morphology and mechanical properties of single-walled carbon nanotubes,” *Chem. Phys. Lett*., **333**, 344–349 (2001).